Solid-State Electronics 128 (2017) 141–147

Contents lists available at ScienceDirect

Solid-State Electronics

journal homepage: www.elsevier.com/locate/sse

Framework to model neutral particle flux in convex high aspect ratio structures using one-dimensional radiosity

Paul Manstetten [a,*], Lado Filipovic [b], Andreas Hössinger [c], Josef Weinbub [a,b], Siegfried Selberherr [b]

[a] Christian Doppler Laboratory for High Performance TCAD, Institute for Microelectronics, TU Wien, Gußhausstraße 27-29/E360, 1040 Wien, Austria
[b] Institute for Microelectronics, TU Wien, Gußhausstraße 27-29/E360, 1040 Wien, Austria
[c] Silvaco Europe Ltd., Compass Point, St Ives, Cambridge PE27 5JL, United Kingdom

ARTICLE INFO

Article history:
Available online 20 October 2016

The review of this paper was arranged by Viktor Sverdlov

Keywords:
High aspect ratio
Neutral particle flux
Etching
Radiosity
View factor

ABSTRACT

We present a computationally efficient framework to compute the neutral flux in high aspect ratio structures during three-dimensional plasma etching simulations. The framework is based on a one-dimensional radiosity approach and is applicable to simulations of convex rotationally symmetric holes and convex symmetric trenches with a constant cross-section. The framework is intended to replace the full three-dimensional simulation step required to calculate the neutral flux during plasma etching simulations. Especially for high aspect ratio structures, the computational effort, required to perform the full three-dimensional simulation of the neutral flux at the desired spatial resolution, conflicts with practical simulation time constraints. Our results are in agreement with those obtained by three-dimensional Monte Carlo based ray tracing simulations for various aspect ratios and convex geometries. With this framework we present a comprehensive analysis of the influence of the geometrical properties of high aspect ratio structures as well as of the particle sticking probability on the neutral particle flux.

1. Introduction

High aspect ratio structures are essential for the fabrication of various semiconductor devices, where the aspect ratio (AR) of the structure is defined as *depth/diameter* in case of cylinders and as *depth/width* in case of trenches. One particular example is negative-AND (NAND) flash cell fabrication [1], where three-dimensional multi-layer designs (3D-NAND) involve vertical holes which require aspect ratios above 40. Significant pressure on control of the fabrication process as well as on modeling and simulation techniques originates from these high aspect ratio structures.

One process to fabricate high aspect ratio structures is ion-enhanced chemical etching (IECE) [2]. In this process, the surface is exposed to reactive atoms and molecules from the plasma, which chemically react with the surface to form a volatile product. However, not only volatile products are created in this reaction, but also non-volatile by-products which hinder subsequent surface reactions and therefore decrease the etch rate. This chemical sealing is frequently desired on the vertical sidewall of high aspect ratio structures. To maintain a high etch rate at the bottom region of a structure, the surface is additionally bombarded with vertically accelerated ions, with the purpose of removing the non-volatile by-products on exposed areas. This makes a highly anisotropic chemical etching possible, supporting the fabrication of high aspect ratio structures.

To simulate an IECE process, a common approach is to model the reactive atoms and molecules of the plasma as electrically neutral particles that diffuse into the domain. In contrast, the accelerated ions are modeled as a directed source. A general simulation sequence for a single time step is to (a) calculate the local neutral particle flux and the local ion flux adsorbed on the surface, (b) model the local surface reaction using the obtained flux rates, and (c) calculate the new surface positions.

Common approaches for three-dimensional flux calculation are Monte Carlo ray tracing [3] and radiosity based [4] methods. When applying these methods to high aspect ratio structures, the computational costs for the neutral flux calculation dominates the simulation. The local neutral flux originating from multiple reflections becomes the dominant component towards the bottom of the structures; this multiplies the computational effort by the number of considered reflection events, compared to the costs for the computation of the direct flux.[1] Also, the flux rates can easily vary by orders of magnitude along the structure depth; this increases the

* Corresponding author.
E-mail address: manstetten@iue.tuwien.ac.at (P. Manstetten).

[1] The flux which originates from direct visibility of the source area.

http://dx.doi.org/10.1016/j.sse.2016.10.029
0038-1101/

number of particles necessary to obtain an acceptable signal-to-noise ratio when using a ray tracing approach. For spatial resolutions typically desired for practical simulation cases, this leads to high computational costs for the full three-dimensional computation of the local neutral flux using Monte Carlo ray tracing or radiosity based methods.

We suggest to use a one-dimensional approximation for the calculation of the local neutral flux inside high aspect ratio structures. Our approach, initially introduced in [5], is radiosity based and is applicable to simulations of convex rotationally symmetric holes and convex symmetric trenches with a constant cross-section.

The adsorption of the neutral particles is modeled with a sticking probability s as a locally constant parameter of the surface. All sources and reflections are treated as ideal diffusive, which is a common assumption for neutral particles [6]. Molecular flow (ballistic transport) is assumed for the neutral particles. The sum of these assumptions allows for the computation of the neutral flux distribution using a radiosity approach, which was originally used in the context of heat transfer [7] and later adopted in computer graphics to compute global illumination [8].

The surface of the structure is discretized into elements along the line of symmetry. Assuming a constant flux and a constant sticking probability s over each surface element, we reformulate the discrete radiosity equation to obtain a *receiving* perspective, which allows for fully adsorbing surface elements.

We establish a general formulation to compute the view factor between two elements of a convex rotationally symmetric hole, based on a formula for the view factor between two coaxial disks of unequal radius. The view factors between two elements of a convex symmetric trench with a constant cross-section is derived using the crossed-strings method [7].

The framework is validated using a three-dimensional Monte Carlo ray tracing based simulator [9] by comparing results for different aspect ratios and sticking probabilities. Furthermore, we study the influence of geometric variations along the wall, as well as the variations of the particle sticking probability, on the flux distribution.

Kokkoris et al. [6] also proposed a framework to approximate the neutral flux in long trenches and holes by exploiting symmetry properties of the structures: The three-dimensional problem is reduced to a line integral and the Nyström method [10] is used for discretization, where a special numerical treatment is needed to avoid singularities. Spikes and oscillations of the solution near corners of the structure were reported, when the resolution is not refined (compared to the resolution required by the Nyström method) at these critical spots. Assumptions for the neutral flux, which are the same for our framework, are the ideal diffuse sources/reflections, the locally constant sticking probability, and molecular flow (ballistic transport without considering inter-particle collisions) of the neutral particles.

In the following sections we first define the simulation domain and introduce the surface model (Section 2). Then, we derive the *receiving* perspective for the discrete radiosity equation (Section 3) and describe the computation of the view factors for holes and trenches (Section 4). Finally, we present the results of the validation and the effects of geometric variations on the wall (Section 5).

2. Simulation domain

For cylindrical holes, the simulation domain is a rotationally symmetric closed convex surface. For trenches, the simulation domain is a trench with a closed convex symmetric cross-section. The neutral flux source is modeled by closing the structures at the top. This leads to a disk-shaped source and a strip-shaped source for holes and trenches, respectively. Fig. 1a and b illustrates the cross-sections of domains with vertical walls and with a kink at one half of the depth, respectively.

The surface adsorption is modeled using a locally constant sticking probability s. The received flux R is split according to s into an adsorbed flux A and a re-emitted flux RE as depicted in Fig. 1c. Source areas additionally emit flux E independent of R.

For the remainder of this work, a sticking probability $s_s = 1$ is used for source areas which to not have any reflections originating from these artificial areas; the bottom is modeled as a fully adsorbing area with a sticking probability $s_b = 1$. A constant sticking probability s_w is used for the walls of the structures. These choices represent a reasonable approximation to the prevalent conditions for the neutral particles in an IECE environment.

3. Radiosity equation

Our assumptions, particularly that all sources and surfaces are ideal diffuse and that the transport of the neutral particles is ballistic, allows for the use of a radiosity formulation.

By assuming a constant flux and a constant sticking probability over each surface element, the problem can be formulated using the discrete radiosity equation: for a surface element i the equation reads

$$B_i = E_i + (1 - \alpha_i)\sum_j (F_{ji} B_j), \tag{1}$$

where B is the radiosity (sum of emitted and reflected energies), E is the self-emitted energy, α is the absorptance, and F_{ji} is the view factor (proportion of the radiated energy, which leaves element j and is received by element i). We adapt (1) to our problem by substituting the absorptance α with the sticking probability s and identifying the adsorbed flux as the adsorbed energy A. The radiosity B is then related to the adsorbed energy A by

$$A_i = (B_i - E_i)\frac{s_i}{1 - s_i}. \tag{2}$$

Since we are also interested in the adsorbed flux at the fully adsorbing areas, (1) and (2) are not applicable because $\lim_{s_i \to 1} A_i = \infty$. For this reason we use the following formulation for the received flux R:

$$R_i = \sum_j (E_j F_{ji}) + \sum_j ((1 - s_j) R_j F_{ji}), \tag{3}$$

where the relation to the adsorbed flux is

$$A_i = R_i s_i. \tag{4}$$

Rewritten in matrix notation and resolved for the vector of the received flux R we obtain

$$\begin{aligned} \mathbf{F}^T \cdot E + \mathrm{diag}(1 - s)\mathbf{F}^T \cdot R &= R, \\ (\mathbf{I} - \mathrm{diag}(1 - s)\mathbf{F}^T) \cdot R &= \mathbf{F}^T \cdot E, \end{aligned} \tag{5}$$

with the vector of emitted flux E, a vector of sticking probabilities s, and a matrix of view factors $\mathbf{F}$ (where F_{ij} corresponds to the view factor $i \to j$).

We approximate the solution of the resulting diagonally-dominant linear system of Eq. (5) using the Jacobi method. Each iteration of the Jacobi method can be imagined as a concurrent diffuse re-emission of each element to all other elements. The adsorbed flux A is obtained by multiplying the entries in the solution for R with the corresponding sticking probability s of the element (4). The relation $\|A\| - \|E\| = 0$, which holds for closed surfaces, can be used to test the implementation and to define a stopping criterion for the Jacobi iterations.

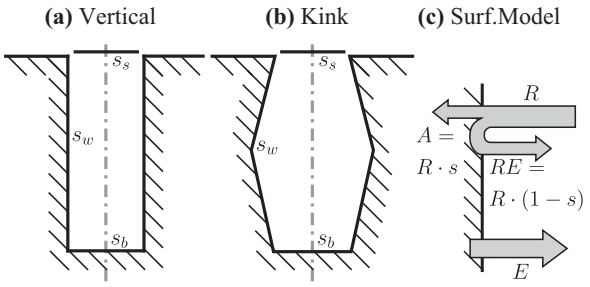

Fig. 1. Cross-sections of simulation domains with vertical walls (a) and with a kink at one half of the depth (b). s_s, s_w, and s_b designate the sticking probabilities for the source, the wall, and bottom region, respectively. (c) Illustrates the surface model showing the relation between the received flux R, the adsorbed flux A, and the re-emitted flux RE; source areas emit flux E independent of the received flux R.

4. View factors

Our approach is based on a discretization of the surface into discrete surface elements along the structure's line of symmetry. Fig. 2 shows the cross-section of a convex structure and the shape of the resulting surface elements. Two vertical ranges are indicated in Fig. 2b and the resulting surface elements a and b are shown for a trench (Fig. 2a) and a hole (Fig. 2c). The elements are formed from two strips for the trench and take the form of a sliced cone for the hole.

To assemble the matrix **F** we need to evaluate the view factors between all possible pairs of surface elements.

4.1. Trench view factors

The view factor between two segments of a symmetric convex trench with a constant cross section, as depicted in Fig. 2a, is derived using the crossed-strings method [7]. This method computes the view factor between two surfaces with a constant cross section and infinite length utilizing a two-dimensional reformulation of the problem. For two mutually completely visible strips of infinite length the view factor is [7]

$$F_{1\to 2} = \frac{(d_1 + d_2) - (s_1 + s_2)}{2 \cdot a_1}, \tag{6}$$

where d_1 and d_2 denote the lengths of the diagonals when connecting the cross-section of the two strips to form a convex quadrilateral, s_1 and s_2 denote the lengths of the sides of that quadrilateral which connects the strips, and a_1 denotes the length of the side of the quadrilateral which represents the emitting strip.

Fig. 3a is an isometric view of the four strips from Fig. 2a. The view factors from the top right strip a_r towards the other three

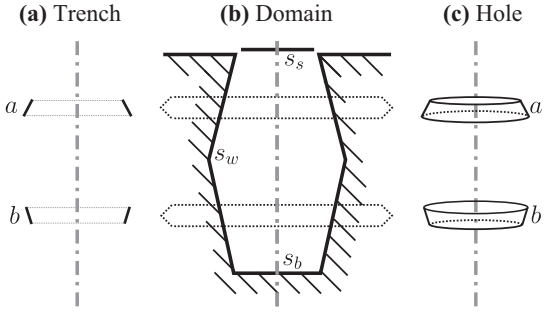

Fig. 2. Two surface elements, which result when discretizing the domain (b) are displayed: (a) is the side view of two surface elements a and b, which result from a trench discretization and (c) is the isometric view of two surface elements a and b, which result form a hole discretization.

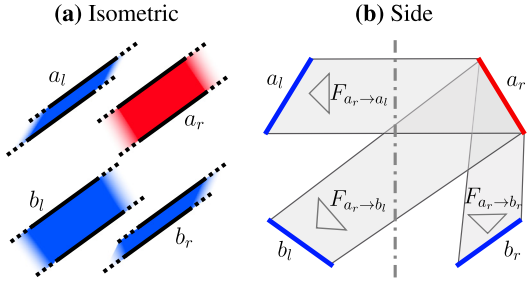

Fig. 3. Isometric (a) and side view (b) on the four infinite strips which correspond to the surface elements a and b from Fig. 2a. In (b), the view factors from the top right strip a_r towards the other three strips are visualized.

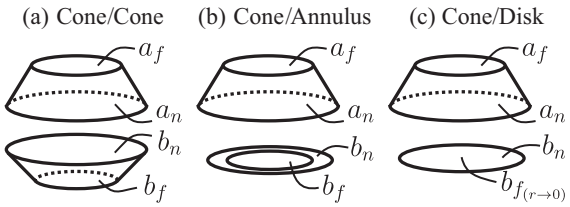

Fig. 4. Three possible pairs of segments as they result from discretizing the hole. For each pair, the near apertures a_n and b_n, and the far apertures a_f and b_f are denoted. (a) Two cone-like segments. (b) Cone and annulus. (c) Cone and disk. The far aperture is treated as an infinitely small element.

strips is visualized in Fig. 3b. The view factor between the two segments a and b is

$$F_{a\to b} = F_{a_r \to b_r} + F_{a_r \to b_l}, \tag{7}$$

where the subscripts denote the side of the strip according to Fig. 3b. a_l can be neglected, as the cross section is symmetric. The view factor of an element to itself is

$$F_{a\to a} = F_{a_r \to a_l}, \tag{8}$$

where again the other direction can be neglected due to symmetry. Eq. (6) is used to compute the view factors between individual strips in (7) and (8).

4.2. Hole view factors

We derive a general formulation to compute the view factors between two segments of a rotationally symmetric convex hole as depicted in Fig. 2c. It is based on the view factor between two coaxial disks of unequal radii r_1 and r_2 at a distance z defined by

$$F_{1\to 2} = \frac{1}{2}\left(X - \sqrt{X^2 - 4(R_1/R_2)^2}\right), \tag{9}$$

where $R_i = r_i/z$ and $X = 1 + (1 + R_2^2)/R_1^2$ [11]. Using this relation and the reciprocity theorem of view factors

$$S_1 \cdot F_{1\to 2} = S_2 \cdot F_{2\to 1}, \tag{10}$$

where S is the element area, we derive a general formulation for the view factor between the inner wall surfaces of two coaxial cone-like segments whose surfaces are mutually completely visible. Fig. 4a shows two segments a and b in such a configuration and denotes the four coaxial disks which represent the apertures of the two elements.

In our formulation, the final goal to compute the view factor between two elements a and b is divided into multiple inexpensive view factor computations between coaxial disks. First, the difference of the view factors from b_f towards the two disks of a is computed, and the reciprocity theorem (10) is applied to obtain F_{ab_f} (red indicates sending and blue receiving areas):

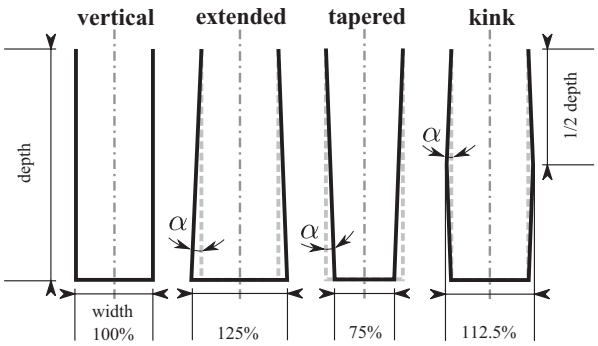

Fig. 5. Cross sections of the geometric variations of the wall for holes and trenches (shown for AR = 3). Starting from a vertical wall, the bottom width is increased by 25% (extended) and reduced by 25% (tapered). Finally, the width at 1/2 of the total depth is increased by 12.5% to form a kink. The resulting angle α, which is identical for all three variations, is depicted.

$$F_{b_f a} = F_{b_f a_n} - F_{b_f a_f} \Rightarrow \frac{S_{b_f}}{S_a} \cdot F_{b_f a} = F_{a b_f} . \tag{11}$$

The same is done for b_n to obtain F_{ab_n}:

$$F_{b_n a} = F_{b_n a_n} - F_{b_n a_f} \Rightarrow \frac{S_{b_n}}{S_a} \cdot F_{b_n a} = F_{a b_n} . \tag{12}$$

Finally F_{ab} is obtained by subtracting F_{ab_f} from F_{ab_n}:

$$F_{a b_n} - F_{a b_f} = F_{ab} . \tag{13}$$

The view factor of an element to itself F_{aa} is computed by subtracting the flux which leaves through the two apertures from unity:

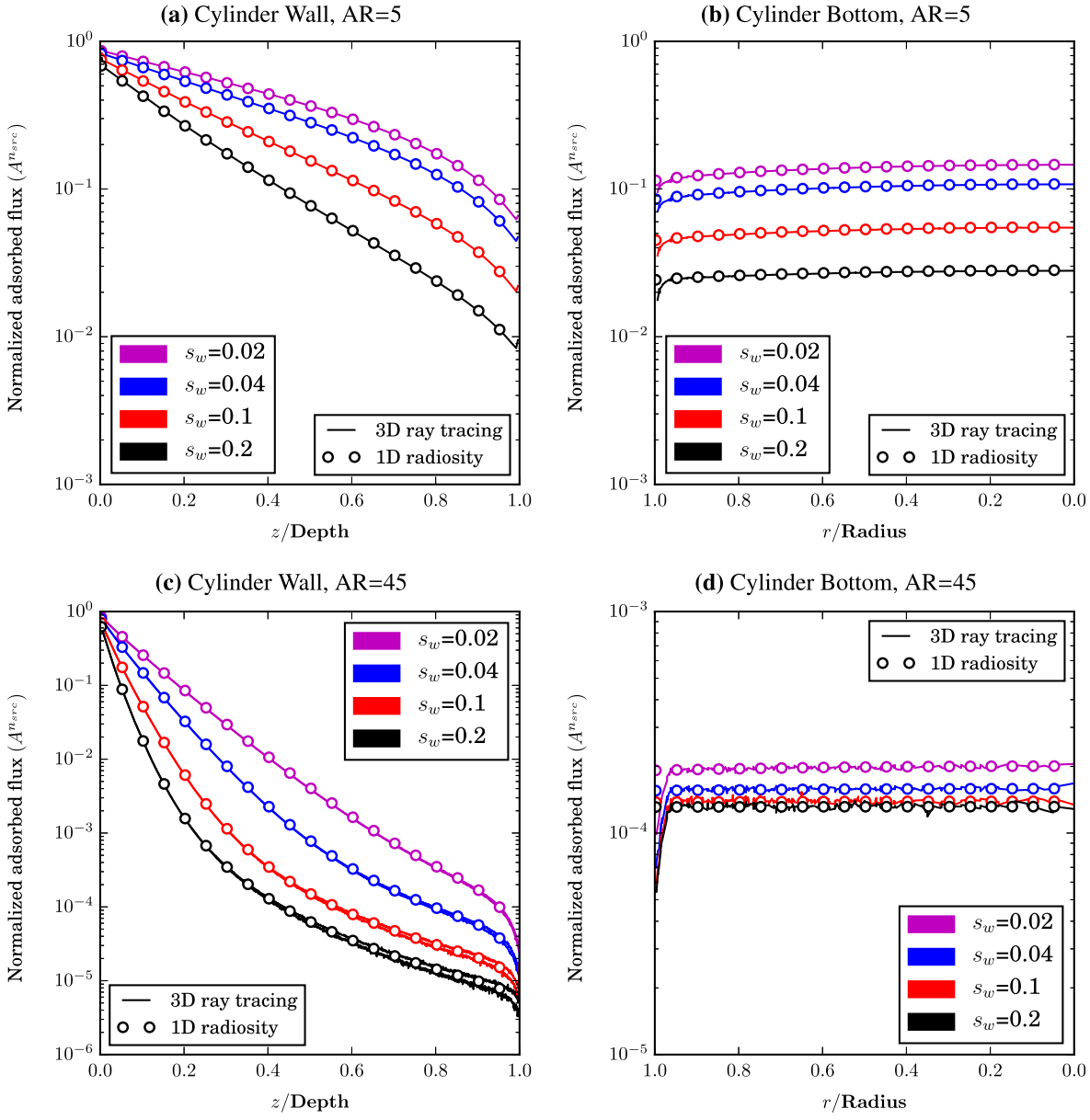

Fig. 6. Normalized flux distributions along the wall and at the bottom for cylinders of aspect ratio 5 (a, b) and aspect ratio 45 (c, d). Our one-dimensional radiosity approach (circles) is compared to a three-dimensional ray tracing simulator (lines). The sticking probability of the wall s_w is varied between 0.02 and 0.2. The deviations between ray tracing and radiosity towards the wall-bottom interface are due to the resolution of the ray tracing simulator. In (c) the ray tracing results are plotted using the minimum and maximum along the cylinder radius, particularly visible for $s_w = 0.2$.

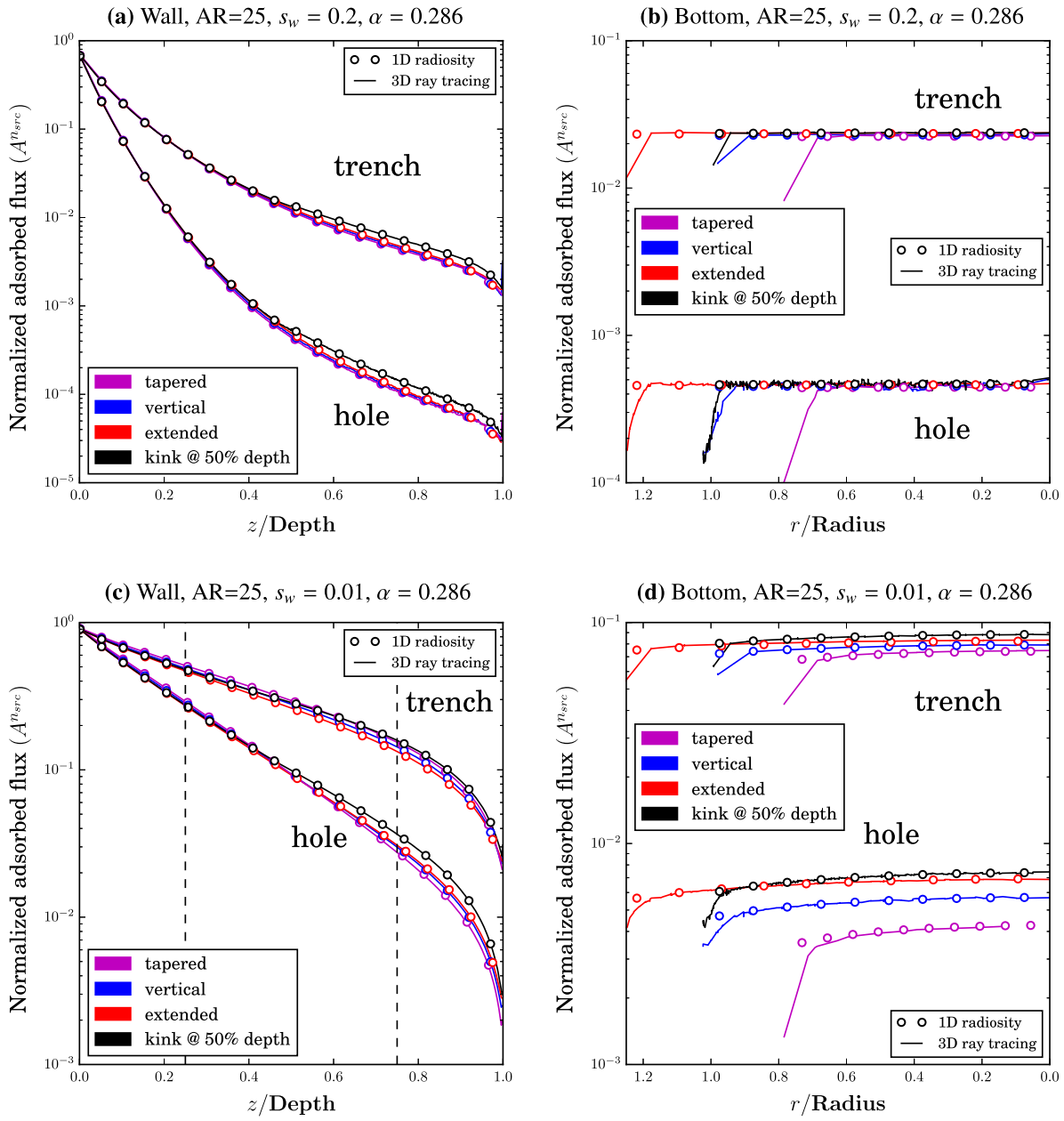

Fig. 7. Normalized flux distributions along the wall and at the bottom of a hole and a trench of AR = 25 for sticking probabilities $s_w = 0.2$ (a, b) and $s_w = 0.01$ (c, d). The geometry of the structures is varied (according to Fig. 5). The results for structures with vertical sidewalls are plotted as a reference. Lines represent the results of the reference ray tracing simulator [9]. The deviations between ray tracing and radiosity towards the wall-bottom interface are due to the limited grid resolution of the ray tracing simulator. The flux distributions at the bottom span the interval [0.75,0] for the tapered structures and [1.25,0] for the extended structures. In (c), the vertical dashed lines mark positions at 25% and 75% of the total depth as a reference for the results in Fig. 8.

$$F_{aa} = 1 - F_{aa_n} - F_{aa_f}. \tag{14}$$

If an element is an annulus or a disk (see Fig. 4b and c, respectively), the general formulation still applies. For a disk, the *far* aperture is treated as an infinitely small element.

5. Results

To provide a good qualitative comparison we normalize the results to only depend on the aspect ratio of the structure and the sticking probability. The adsorbed flux A is divided by the area of the element ($A_i^n = A_i/S_i$) and normalized to the flux which a surface of the same sticking probability would absorb, if it is fully planar-exposed to the source ($A_i^{n_{src}} = A_i^n / E_{i_{src}}^n \cdot S_i$).

The sticking probabilities of the source areas at the top s_s and the bottom of the structures s_b are modeled as fully adsorbing in all of the following results.

5.1. Validation: cylindrical holes

To evaluate the quality of our one-dimensional radiosity model, we analyze different simulation setups of cylinders, where we vary the sticking probability of the wall between $s_w = 0.02$ and $s_w = 0.2$. Fig. 6a and b compares the flux distributions for structures where AR = 5 obtained using the proposed one-dimensional radiosity approach with results generated with a reference Monte Carlo ray tracing tool [9]. Similarly, Fig. 6c and d compares the flux distributions for structures where AR = 45. The results show a good agreement, aside from the deviation at the wall/bottom interface,

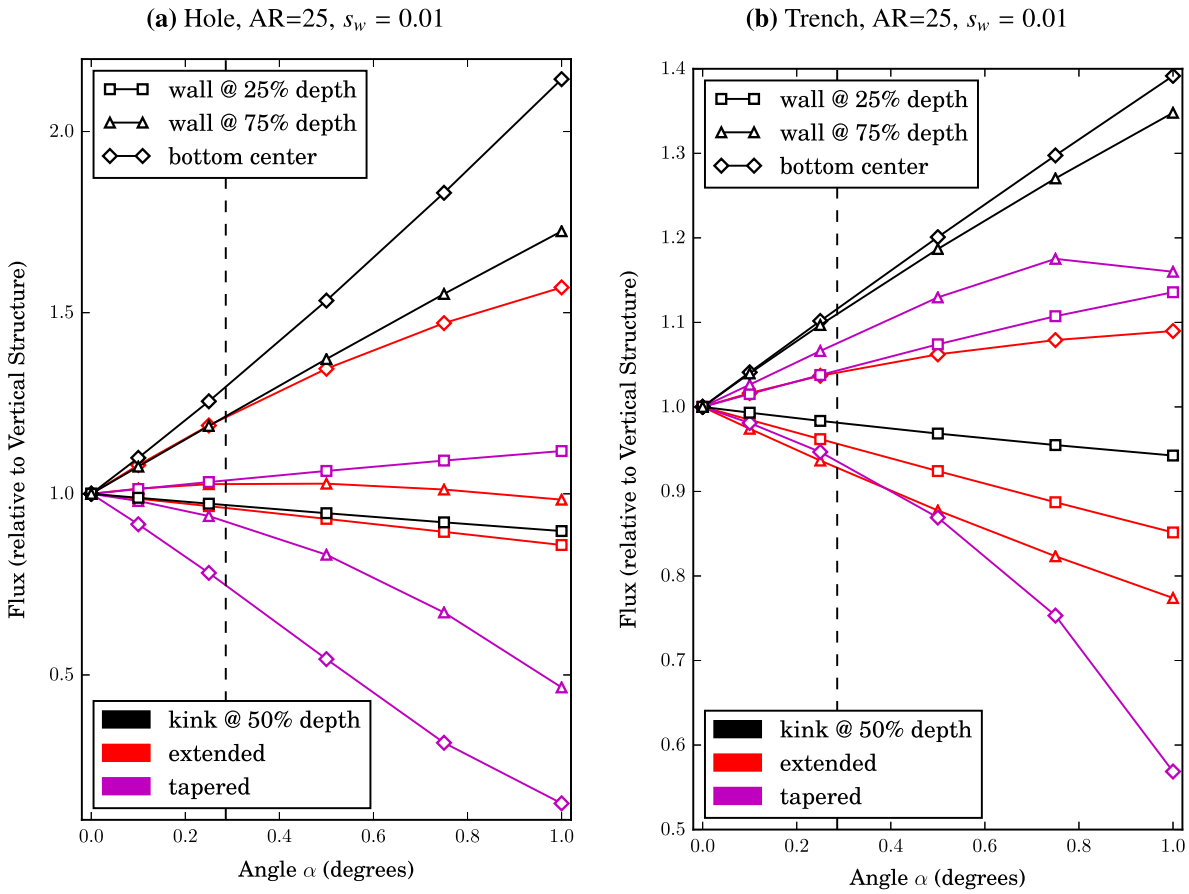

Fig. 8. Flux in a convex hole (a) and trench (b) (with tapered, extended, and kinked sidewalls) relative to the flux in a hole and a trench with vertical walls for an aspect ratio 25 and a wall sticking probability $s_w = 0.01$. The flux at the bottom center and at two points on the wall (at 25% and 75% of the total depth) is plotted over the angle α (introduced in Fig. 5). The angle α corresponds to the taper angle (tapered), the extension angle (extended), and to the angle which is formed by a kink at one half of the total depth of the structure. The vertical dashed lines indicate an angle $\alpha = 0.286°$ as a visual reference to the results in Fig. 7c.

caused by the discretization which is used in the ray tracing simulation. In Fig. 6c two flux distributions are plotted for the ray tracing results along the wall; they represent the minimum and maximum along the cylinder radius. The separation of the flux distributions, particularly visible for $s_w = 0.2$ (Fig. 6c), and the visible noise in Fig. 6d, reflect the stochastic nature of the ray tracing approach.

5.2. Validation: convex structures

To validate our method for convex structures, several geometric variations including an extended, tapered, and kinked sidewall, visualized in Fig. 5, are applied to a hole and a trench of aspect ratio 25. Good agreement is achieved when comparing to the results obtained with a reference Monte Carlo ray tracing simulator.

Furthermore, the results allow to study the influence of the geometrical properties of high aspect ratio structures as well as of the particle sticking probability on the neutral particle flux. Fig. 7 compares the resulting flux distributions along the wall and at the bottom for sticking probabilities $s_w = 0.2$ and $s_w = 0.01$. For a sticking probability $s_w = 0.2$, Fig. 7a and b shows small variations along the wall and at the bottom for both, holes and trenches. Solely the presence of the kink clearly increases the flux on the bottom half of the wall.

When decreasing the sticking probability to $s_w = 0.01$, Fig. 7c indicates stronger deviations along the entire wall for all geometries. Fig. 7d reveals a variation of about ±25% and ±10% for the bottom flux in a hole and a trench, respectively.

To summarize, low sticking probabilities increase the influence of geometric variations on the flux distributions along the wall, and especially at the bottom of high aspect ratio structures.

5.3. Variation of wall geometries

Using our framework, the influence of the wall geometry on the flux distributions is studied in more detail using a hole and a trench of aspect ratio 25 with a wall sticking probability $s_w = 0.01$. For $\alpha = 0.286°$, this reassembles the configuration used to produce the results in Fig. 7c and d. Fig. 8 compares the flux at the bottom center and two points on the wall (at 25% and 75% of the depth) when additionally varying α (depicted in Fig. 5) from 0° to 1°.

For the kinked structures, the angular dependence of the flux at all three positions can be approximated with a linear relation to the flux in a structure with vertical sidewalls. The results for the extended and especially the tapered structures reveal the generally non-linear relation already for small angles. Fig. 8a and b shows that the kinked sidewall leads to higher flux rates at the bottom, compared to the extended configuration; the tapered configuration reduces the bottom flux.

When interpreting the results, it must be considered that the fully adsorbing bottom area changes its size when tapering or extending the structure. For $\alpha = 1°$, the bottom width/diameter is reduced to 13% and extended to 187%, for the tapered and extended structures, respectively. This is likely one reason why

the bottom flux is, at all angles, higher for the kinked structures, when comparing with the extended structures.

6. Summary and outlook

We provide an approximation of the local neutral flux in three-dimensional plasma etching simulations of high aspect ratio holes and trenches, using a one-dimensional radiosity approach. The radiosity equation is reformulated into a *receiving* perspective, which allows to model fully adsorbing surface elements. We compute all relevant view factors for holes by establishing an inexpensive general formulation for the view factor between coaxial cone-like segments. Comparing the results for various convex configurations using a rigorous three-dimensional Monte Carlo ray tracing simulation good agreement is noted and the applicability of our model for practical situations is confirmed.

We study the influence of geometric variations on the wall as well as the sticking probability on the flux distributions. The results indicate a strong influence for low sticking probabilities which are typical in IECE simulations of high aspect ratio structures. The influence is studied in more detail for holes and trenches using a sticking probability $s_w = 0.01$ and an aspect ratio of 25. The results provide a compact overview on the magnitude of the flux deviation at different positions in the structure, when comparing to the idealized shape.

Our framework is based on a computationally inexpensive and straightforwardly implementable method to compute the neutral flux distributions inside convex symmetric holes and convex symmetric trenches of constant cross-section. It can be used as a drop-in replacement for the neural flux computation during three-dimensional IECE simulations of high aspect ratio structures to significantly reduce simulation times in practical simulation cases – or as a stand-alone tool which provides fast results for general investigations.

Acknowledgments

The financial support by the *Austrian Federal Ministry of Science, Research and Economy* and the *National Foundation for Research, Technology and Development* is gratefully acknowledged.

References

[1] Dimitrakis P. Charge-trapping non-volatile memories. Basic and advanced devices, vol. 1. Springer; 2015.
[2] Francis JPC, Chen F. Lecture notes on principles of plasma processing. Springer; 2003.
[3] Ertl O, Selberherr S. Three-dimensional level set based bosch process simulations using ray tracing for flux calculation. Microelectron Eng 2010;87(1):20–9.
[4] Ikeda T, Saito H, Kawai F, Hamada K, Ohmine T, Takada H, et al. Development of SF_6/O_2/Si plasma etching topography simulation model using new flux estimation method. In: Proceedings of the international conference on simulation of semiconductor processes and devices (SISPAD). p. 115–8.
[5] Manstetten P, Filipovic L, Weinbub J, Hössinger A, Selberherr S. Using one-dimensional radiosity to model neutral particle flux in high aspect ratio holes. In: Joint international EUROSOI workshop and international conference on ultimate integration on silicon (EUROSOI-ULIS). IEEE; 2016. p. 120–3.
[6] Kokkoris G, Boudouvis AG, Gogolides E. Integrated framework for the flux calculation of neutral species inside trenches and holes during plasma etching. J Vac Sci Technol A 2006;24(6):2008–20.
[7] Modest MF. Radiative heat transfer. Academic Press; 2013.
[8] Philip D, Kavita B, Philippe B, Peter S. Advanced global illumination. AK Peters Ltd; 2006.
[9] Ertl O, Filipovic L, Weinbub J, Vienna TS; 2015. <https://github.com/viennats/viennats-dev>.
[10] Nyström EJ. Über die praktische Auflösung von Integralgleichungen mit Anwendungen auf Randwertaufgaben. Acta Math 1930;54(1):185–204.
[11] Howell JR, Menguc MP, Siegel R. Thermal radiation heat transfer. CRC Press; 2010.